

Dynamic behaviour of a high-strength structural steel at low temperatures

Maria Jesus Perez-Martin^{a,b,*}, Jens K. Holmen^{a,b}, Susanne Thomesen^b, Odd S. Hopperstad^{a,b} and Tore Børvik^{a,b}

^a Centre for Advanced Structural Analysis (CASA), Norwegian University of Science and Technology (NTNU), NO-7491 Trondheim, Norway

^b Structural Impact Laboratory (SIMLab), Department of Structural Engineering, NTNU, NO-7491 Trondheim, Norway

Abstract

The main objective of this [experimental](#) study is to determine the effect of low temperatures on the mechanical behaviour of Strenx 960 Plus high-strength structural steel at different strain rates [and stress triaxialities](#). For this purpose, a comprehensive experimental campaign was designed to characterise the material at a wide range of temperatures and loading rates. [The stress triaxiality was varied by testing specimens with different geometry](#). First, to determine the ductile-to-brittle transition temperature, instrumented Charpy V-notch impact tests were carried out at a range of temperatures from +20°C down to -90°C. The impact energy dropped gradually with decreasing temperature, [but](#) a clear transition temperature could not be identified. A fractography study exhibited a clear dimple structure, revealing predominantly ductile fracture at all temperatures. Then, uniaxial tension tests on smooth and pre-notched axisymmetric specimens under both quasi-static and dynamic loading rates were carried out at room temperature and low temperatures. [These tests were conducted to characterise the rate-dependence of the stress-strain behaviour and the failure strain](#). The results revealed that under quasi-static conditions the flow stress increased with decreasing temperature, while the failure strain was nearly independent of the temperature. Dynamic tensile tests using the same specimen geometries were conducted in a split

* Corresponding author.

Email-address: mariajesus.perez@ntnu.no (Maria Jesus Perez-Martin)

26 Hopkinson tension bar at +20°C and −40°C. The material exhibited a positive strain rate
27 sensitivity at all investigated temperatures. This experimental study reveals that the Strenx
28 960 Plus steel retains its ductility at temperatures as low as −40°C. Brittle failure could not
29 be observed even with combined high strain rate, high stress triaxiality and low temperature.

30 **1. Introduction**

31 The amount of human activity in the Arctic region is increasing. Average Arctic winter
32 temperatures can be as low as −40°C, which means that Arctic structures are installed and
33 operated at extreme temperatures and sometimes subjected to severe loading conditions. At
34 high temperatures, steels are generally ductile. As the ambient temperature decreases, many
35 steels become vulnerable to brittle fracture and may not be suitable for cold climate
36 applications. Consequently, there has been a number of studies on structural steels exposed
37 to Arctic environments in recent years [1-8].

38 Ductile fracture in metals is characterised by void nucleation, growth and coalescence.
39 Failure is a result of the voids growing to a critical size and the development of a local
40 plastic instability. Brittle fracture is characterised by an abrupt and unexpected initiation
41 and propagation of fracture along a particular crystallographic plane. Cleavage is a typical
42 brittle failure, but it might also be preceded by large-scale plastic flow and ductile crack
43 growth. Dieter [9] stated that there are three basic factors contributing to cleavage: a triaxial
44 stress state, low temperature and high strain rate. According to Anderson [10], cleavage is
45 most likely to occur when the plastic flow is restricted.

46 In general, face-centred cubic (FCC) metals, like aluminium, are not susceptible to
47 cleavage due to the large amount of slip systems at all temperatures. On the other hand,
48 body-centred cubic (BCC) metals, like steel, have few active slip systems when the
49 temperature becomes sufficiently low and may therefore fail by cleavage. The fracture
50 mechanism of BCC metals may change radically from ductile to brittle at a small sub-zero

51 temperature range. This is called the ductile-to-brittle transition temperature (DBTT), or the
52 transition temperature, which is affected by the chemical composition and the
53 microstructure. According to Dieter [9], the best combination of strength and impact
54 resistance in steel is given by a tempered martensitic structure. In practical applications and
55 for design purposes particularly in Arctic environments, it is important to be aware of the
56 potential transition from ductile to brittle behaviour.

57 A widely used method to determine the DBTT is the Charpy V-notch impact test [11],
58 in which a heavy pendulum strikes a notched specimen to fracture. Tests are conducted over
59 a wide temperature range, and the energy absorption is plotted as a function of temperature.

60 The effect of elevated temperatures on the mechanical behaviour of metals is well
61 known in both quasi-static and dynamic conditions [12, 13]. In general, the strength of
62 metallic materials decreases, and the fracture strain increases with increasing temperature.
63 However, the behaviour of such materials at low temperatures has not been extensively
64 studied, at least not in an impact engineering context. In a recent study by Tu et al. [14], a
65 structural steel exhibited increased strength without losing ductility at temperatures as low
66 as -60°C . However, this investigation was conducted under quasi-static loading conditions
67 and the effect of high strain rates at low temperatures was not studied. Similar results were
68 found by Xie et al. [7] on the mechanical properties of high-strength steel wires. In that
69 study, the ultimate strength and failure strain of the material increased as the temperature
70 dropped from $+20^{\circ}\text{C}$ down to -100°C , while brittle fracture was observed at temperatures
71 below -100°C .

72 The current study presents material tests using several different specimens and strain
73 rates to investigate how a commercial high-strength steel behaves at sub-zero temperatures
74 relevant for Arctic applications. All the results are compared to corresponding tests at room
75 temperature. Special emphasis is put on the fracture behaviour.

76 **2. Material**

77 *2.1. Material description*

78 The material used in the current study is the hot-rolled, quenched and tempered strip
79 steel Strenx 960 Plus which was produced and provided by Swedish Steel AB (SSAB). It is
80 a high-strength martensitic steel typically employed for demanding load-bearing structural
81 applications, where the number indicates that the material has a minimum yield strength of
82 960 MPa. The chemical composition, both from a ladle analysis and the certificate, as well
83 as nominal mechanical properties of the Strenx 960 Plus provided by the supplier, are
84 summarised in Table 1. According to the material certificate, the absorbed impact energy in
85 a Charpy test is at least 27 J at -40°C .

86 *2.2. Specimen geometries*

87 The experimental program included the following tests:

- 88 • Smooth and pre-notched tensile specimens subjected to quasi-static and dynamic
89 loading rates at room and low temperatures.
- 90 • Charpy V-notch impact tests at room and low temperatures.

91 Smooth round bars and axisymmetric notched tensile specimens were machined from an 8
92 mm thick Strenx 960 Plus steel plate. The geometries of the smooth and pre-notched
93 specimens with different notch-root radii are shown in Figure 1(a), (b) and (c). To study the
94 anisotropy of the material, the smooth specimens were extracted from three different
95 orientations with respect to the rolling direction of the plate: 0° , 45° and 90° , with 0° being
96 the rolling direction. The pre-notched specimens, with radius $R = 2.0$ mm (R2.0) and $R =$
97 0.8 mm (R0.8), were only extracted from the rolling direction. Before testing, the minimum
98 cross-section diameter of each specimen was measured with a laser gauge.

99 The geometry of the Charpy V-notch specimens is shown in Figure 1(d). The red line
100 on the cross-section indicates the thickness direction of the 8 mm thick steel plate. The sub-
101 standard geometry of the specimens was in accordance with the relevant standards [15].

102 **3. Experimental procedures**

103 A comprehensive experimental campaign was designed to characterise the Strenx 960
104 Plus steel at a wide range of temperatures and loading rates. First, instrumented Charpy V-
105 notch impact tests were conducted *in an attempt* to determine the ductile-to-brittle transition
106 temperature. *Then, to characterise the rate-dependence of the stress-strain behaviour and*
107 *the failure strain*, experiments on smooth and pre-notched tension specimens were carried
108 out under both quasi-static and dynamic loading rates at room and low temperatures. In
109 general, two or three repetitions were conducted for each specimen geometry and type of
110 test. *An exception is the dynamic tensile tests at room temperature on pre-notched*
111 *specimens with radius R2.0 where only one test was successful.*

112 *3.1. Charpy V-notch tests*

113 Charpy V-notch tests were carried out according to the ISO 148-1:2016 standard using
114 an inverse setup (see Figure 2) [16]. In an inverse setup, the specimen is attached to a 21 kg
115 pendulum with an 800 mm long arm that impacts what is usually known as the striker.
116 *Before testing, the specimens were cooled down in an alcohol bath to the desired test*
117 *temperatures of +20°C, -20°C, -40°C, -60°C, -75°C or -90° for at least 10 minutes. Then,*
118 *each specimen was rapidly transferred to the impact position and impacted by the striker,*
119 *the elapsed time being not more than 5 s.*

120 *3.2. Quasi-static tensile tests*

121 The quasi-static tensile tests were conducted in a Zwick Roell Z030 electromechanical
122 testing machine equipped with a 30 kN load cell. The crosshead velocity of the test machine

123 was specified to 0.15 mm/min, giving an initial strain rate in the smooth specimens of
124 $5 \times 10^{-4} \text{ s}^{-1}$. This strain rate corresponds to quasi-static conditions, even though the strain
125 rate will increase as the specimen deforms. The tests were recorded with a digital camera
126 configured to achieve 3 fps with a resolution of 2448×2048 pixels. A 2-plane mirror system
127 allowed recording the specimen on two orthogonal planes, using a LED light system to
128 improve the grey-scale gradient between the specimen and the background. An optical edge-
129 tracing technique [17, 18], implemented in the software eCorr [19], was used to monitor the
130 minimum cross-section diameter of the specimen in two perpendicular directions (see
131 Figure 3(a)). With this technique, the gradient in grey-scale value of the specimen towards
132 the background is used to define the edge and subsequently the minimum diameter of the
133 specimen during loading. The edge-tracing technique was validated against DIC in [17],
134 showing good agreement.

135 To study the in-plane anisotropy of the material, smooth tension specimens extracted
136 at 0° , 45° and 90° with respect to the rolling direction of the steel plate were tested at room
137 temperature. Tensile tests of smooth and pre-notched ($R = 2.0 \text{ mm}$ and $R = 0.8 \text{ mm}$)
138 specimens extracted from the rolling direction were performed at $+20^\circ\text{C}$ and -40°C . The
139 tests at low temperature were conducted in a temperature chamber where the specimens
140 were cooled down using liquid nitrogen. The chamber was equipped with a window through
141 which the test specimen could be recorded (see Figure 3(b)). After having reached the
142 desired level, the temperature was held constant for at least 20 minutes to ensure no
143 temperature gradients throughout the specimen. This was done by flushing liquid nitrogen
144 into the chamber in a controlled way based on thermocouple measurements (see also Section
145 3.3). Three thermocouples were installed inside the chamber. Two of them were spot-
146 welded to the machine grips, while the third was located close to the centre where the

147 specimen was held. In this way, they allowed to control the amount of liquid nitrogen
148 flushed into the chamber to keep a constant temperature for a long time.

149 3.3. *Dynamic tensile tests*

150 Dynamic tensile tests using the same specimen geometries as in the quasi-static tests
151 were conducted in a split Hopkinson tension bar (SHTB) at +20°C and -40°C. The
152 experimental set-up [20], schematically illustrated in Figure 4(a), was composed of an input
153 bar (AC) and an output bar (DE), both made of steel quality Tibnor 52SiCrNi5. A friction
154 locking mechanism (B), which clamped the input bar, allowed the stress wave to be
155 generated. The specimen was mounted between C and D. The SHTB was equipped with
156 strain gauges at each of the positions ①, ② and ③. Strain gauges ② and ③ were used to
157 determine the stress in the specimen, while gauge ① was used to monitor the tension force
158 N_0 used to strain the input bar. Using the signals from the strain gauge measurements, the
159 nominal stress, nominal strain and nominal strain rate in the sample can be obtained based
160 on one-dimensional stress wave theory (see [20] for details).

161 In these experiments, the force was obtained based on the transmitted stress wave,
162 while the current cross-section diameter of each specimen was monitored using a Phantom
163 V1610 high-speed camera and edge tracing. The camera was set up to record 240,000 fps,
164 leading to a time increment of 4.17 μ s between consecutive images, and with a resolution
165 of 256×208 pixels. In order to perform the tests at low temperature of -40°C, the specimen
166 was located in a purpose-built temperature chamber made of polycarbonate to ensure
167 visibility while being cooled down with liquid nitrogen flushed into the chamber (see Figure
168 4(b) and (c)). To avoid condensation on the surface of the specimen, they were carefully
169 cleaned with isopropyl alcohol before the tests. Three thermocouples were utilised to
170 measure and control the sub-zero temperature: two of them were spot-welded to the bars
171 near the specimen, while the third thermocouple was placed freely inside the chamber. It

172 should be noted that there was only one successful test of the dynamic tensile test at -40°C
173 on the pre-notched specimen R2.0.

174 **4. Experimental results**

175 *4.1. Charpy V-notch tests*

176 The absorbed energy in the Charpy V-notch tests as a function of temperature, from
177 $+20^{\circ}\text{C}$ down to -90°C , is shown in Figure 5(a). Note that the measured absorbed energy at
178 -40°C is significantly higher than the minimum value given by the material certificate (see
179 Table 1). The results revealed that the absorbed energy gradually decreased with decreasing
180 temperature. However, contrary to what one would expect to observe in a typical steel with
181 a DBTT, no clear drop in energy absorption at a specific temperature could be identified.
182 According to Dieter [9], the shape of the temperature-transition curve highly depends on the
183 material (see Figure 5(b)). FCC and most HCP materials have such high notch toughness
184 that brittle fracture is normally not a problem. On the contrary, BCC materials (such as
185 steels) have much lower notch toughness. Thus, brittle fracture is in principle possible at all
186 temperatures and strain rates. The notch toughness of low- and medium-strength BCC
187 materials is strongly dependent on the temperature. At low temperature, fracture occurs by
188 cleavage while at high temperature the fracture occurs by ductile rupture, and the
189 temperature-transition curve may be abrupt. Furthermore, important changes in the
190 transition temperature can be produced by changes in the chemical composition or the
191 microstructure of mild steels. For high-strength steels, such as the Strenx 960 Plus
192 investigated here, the transition temperature is as seen less distinct.

193 *4.2. Quasi-static tensile tests*

194 In the quasi-static tensile tests, the force F was measured by the calibrated load cell,
195 while the minimum cross-section diameters of the specimen in two perpendicular directions,

196 denoted D_1 and D_2 , were provided using edge tracing (see Section 3.2). As these test
197 specimens were axisymmetric (see Figure 1), the initial and current cross-section areas were
198 calculated from $A_0 = \frac{\pi}{4} D_0^2$ and $A = \frac{\pi}{4} D_1 D_2$, respectively, where D_0 is the initial diameter
199 of the specimen. The true stress σ and the logarithmic strain ε were then calculated as

$$200 \quad \sigma = \frac{F}{A}, \quad \varepsilon = \ln\left(\frac{A_0}{A}\right)$$

201 Note that the true stress and logarithmic strain are average values over the minimum cross-
202 section of the specimen after diffuse necking, and that plastic incompressibility and small
203 elastic strains were assumed to obtain the logarithmic strain.

204 Obtained true stress-strain curves corresponding to the smooth specimens extracted
205 from three different orientations (0° , 45° and 90° with respect to the rolling direction) and
206 tested at room temperature are shown in Figure 6(a). These experimental results confirm
207 that the stress-strain response is rather isotropic, even though minor differences in both flow
208 stress and strain to failure are seen between the different specimen orientations.

209 Figure 6(b) shows true stress-strain curves of smooth and pre-notched specimens
210 extracted from the rolling direction and tested at both $+20^\circ\text{C}$ and -40°C . The results
211 revealed that for all the specimen geometries the flow stress increased with decreasing
212 temperature, while the failure strain remained almost the same. Similar results on a 420 MPa
213 structural steel were found by Tu et al. [14], where the fracture strain did not deteriorate
214 when the temperature decreased from room temperature down to -60°C .

215 4.3. Dynamic tensile tests

216 The initial strain rate in the dynamic tensile tests of smooth specimens was between
217 100 and 1000 s^{-1} , and the strain rate increased significantly after necking. Due to the initial
218 notch, the strain rate in the pre-notched specimen tests was never constant. Since there was
219 no apparent relationship between flow stress and strain rate, and since the variation of strain

220 rate was less than an order of magnitude, all the dynamic tensile tests were treated as a single
221 data set.

222 As it can be seen in Figure 7(a), the stress level increased with increasing strain rate,
223 being slightly higher at low temperature, i.e., -40°C , than at room temperature (see Figure
224 7(b)). The Strenx 960 Plus exhibited positive strain rate sensitivity, which was roughly the
225 same at room temperature and low temperature. *It should be noted that, although two or
226 three repetitions within each test series were performed, only a representative stress-strain
227 curve for each geometry is shown in Figure 6 and Figure 7.*

228 **5. Fractographic study**

229 A fracture surface topography analysis was performed on some representative
230 specimens to study the fracture mechanisms. The fracture surfaces were examined with a
231 Zeiss Gemini SUPRA 55 VP FESEM. A first microstructural analysis of the material
232 revealed a pure martensitic structure of the Strenx 960 Plus with a grain size of
233 approximately $10 - 20 \mu\text{m}$.

234 Cleavage fracture is typically represented by a multifaceted surface and ‘river patterns’
235 on each facet of the Charpy specimen [10]. None of these characteristics were observed on
236 the fracture surfaces resulting from the Charpy tests. A clear dimple structure was seen on
237 the fracture surface of the Charpy V-notch specimens; although delamination was more
238 prominent at lower temperatures, as can be observed in Figure 8. *It is believed that the
239 higher stress level in the material at -40°C is the main contributing factor to the greater
240 tendency of delamination.*

241 A classic dimple structure was observed on the tension specimen surfaces at all
242 temperatures, indicating ductile failure. More shallow dimples could be observed on the
243 fracture surface of pre-notched tension specimens (see Figure 9), indicating less ductile
244 behaviour. This effect was experimentally confirmed and could be observed in Figure 6(b),

245 where the strain to failure decreased while the stress triaxiality increased because of the
246 introduction of the notch.

247 As it can be seen in Figure 10, dimples were shallower with decreasing temperature.
248 One may assume that shallow dimples imply less ductile material behaviour. However, a
249 reduction of strain to failure due to decreasing temperature could not be experimentally
250 observed in Figure 6(b). The shallower dimples observed at -40°C could be a delayed void
251 formation due to low temperatures.

252 Delamination was observed on all the specimens tested at both room temperature and
253 -40°C . It can be seen as the cracks, which are perpendicular to the thickness direction of
254 the smooth tension specimen in Figure 11(a). Also, a large crack perpendicular to the
255 thickness direction was observed in the centre of the notched specimens (see Figure 11(b)).
256 Similar cracks were observed by Manes et al. [21] on a pipeline steel. A possible reason
257 they found was the relatively large tensile stresses induced by the strong necking in the
258 thickness direction that lead to secondary cracks along the rolling plane of the material.

259 **6. Conclusions**

260 This experimental study showed that Strenx 960 Plus high-strength structural steel
261 retained its ductility at temperatures as low as -40°C . Fractography revealed only dimple
262 dominated ductile failure, thus brittle failure was not observed in any of the tests, not even
263 in tests with combined high strain rate, high stress triaxiality and low temperature. The strain
264 rate sensitivity was positive at room temperature as well as at sub-zero temperatures. This
265 high-strength structural steel may therefore be a suitable material for use in protective
266 structures in Arctic environments. *However, it remains to check if an evoked fatigue crack,
267 created to significantly increase the stress triaxiality at the crack tip, will alter this
268 conclusion.*

269 **Acknowledgments**

270 The present work has been carried out with the financial support from Centre for Advanced
271 Structural Analysis (CASA) through the Research Council of Norway's Centre for Research
272 based Innovation (CRI) scheme (project 237885). Thankful acknowledgements are made to
273 Tore A. Kristensen at SINTEF Industry and Trond Auestad at Department of Structural
274 Engineering, NTNU, for assistance with the various experimental programmes.

275

276 **References**

- 277 [1] S. Ehlers, E. Østby, Increased crashworthiness due to arctic conditions – The influence of sub-
278 zero temperature, *Marine Structures* 28(1) (2012) 86-100.
- 279 [2] P. Layus, P. Kah, V. Ryabov, J. Martikainen, Evaluation of applicability of thick E500 TMCP
280 and F500W QT steel plates for Arctic service, *International Journal of Mechanical and Materials*
281 *Engineering* 11(1) (2016) 4.
- 282 [3] W. Nam, J. Amdahl, O.S. Hopperstad, Influence of brittle fracture on the crashworthiness of ship
283 and offshore structures in Arctic conditions, 7th International Conference on Collision and
284 Grounding of Ships and Offshore Structures (ICCGS 2016), 2016.
- 285 [4] J.K. Paik, B.J. Kim, D.K. Park, B.S. Jang, On quasi-static crushing of thin-walled steel structures
286 in cold temperature: Experimental and numerical studies, *International Journal of Impact*
287 *Engineering* 38(1) (2011) 13-28.
- 288 [5] D.K. Park, K.J. Kim, J.H. Lee, B.G. Jung, X. Han, B.J. Kim, J.K. Seo, Y.C. Ha, J.K. Paik, T.
289 Matsumoto, S.H. Byeon, M.S. Kim, Collision Tests on Steel-Plated Structures in Low Temperature,
290 ASME 2015 - 34th International Conference on Ocean, Offshore and Arctic Engineering, 2015.
- 291 [6] K. Valtonen, V. Ratia, K.R. Ramakrishnan, M. Apostol, J. Terva, V.-T. Kuokkala, Impact wear
292 and mechanical behavior of steels at subzero temperatures, *Tribology International* 129 (2019) 476-
293 493.
- 294 [7] J. Xie, X. Zhao, J.-B. Yan, Mechanical properties of high strength steel strand at low
295 temperatures: Tests and analysis, *Construction and Building Materials* 189 (2018) 1076-1092.
- 296 [8] J. Xie, G.-R. Zhu, J.-B. Yan, Mechanical properties of headed studs at low temperatures in Arctic
297 infrastructure, *Journal of Constructional Steel Research* 149 (2018) 130-140.
- 298 [9] G.E. Dieter, *Mechanical Metallurgy*, 3rd ed. ed., Mc Graw-Hill Book Co., New York, 1986.
- 299 [10] T.L. Anderson, *Fracture mechanics: fundamentals and applications*, CRC press 2005.

- 300 [11] M.A. Meyers, K.K. Chawla, Mechanical Behavior of Materials, Second Edition ed.,
301 Cambridge2008.
- 302 [12] V. Vilamosa, A.H. Clausen, E. Fagerholt, O.S. Hopperstad, T. Børvik, Local Measurement of
303 Stress–Strain Behaviour of Ductile Materials at Elevated Temperatures in a Split-Hopkinson
304 Tension Bar System, Strain 50(3) (2014) 223-235.
- 305 [13] B. Erice, F. Gálvez, D.A. Cendón, V. Sánchez-Gálvez, Flow and fracture behaviour of FV535
306 steel at different triaxialities, strain rates and temperatures, Engineering Fracture Mechanics 79
307 (2012) 1-17.
- 308 [14] S. Tu, X. Ren, T.A. Kristensen, J. He, Z. Zhang, Study of low-temperature effect on the fracture
309 locus of a 420-MPa structural steel with the edge tracing method, Fatigue and Fracture of
310 Engineering Materials and Structures 41(8) (2018) 1649-1661.
- 311 [15] ISO, Metallic materials -- Charpy pendulum impact test -- Part 1: Test method, ISO 148-1:2016.
- 312 [16] ISO, Metallic materials -- Charpy pendulum impact test -- Part 2: Verification of testing
313 machines, ISO 148-2:2016.
- 314 [17] E. Fagerholt, Field measurements in mechanical testing using close-range photogrammetry and
315 digital image analysis, NTNU, Trondheim, Norway, 2012.
- 316 [18] S. Thomesen, O.S. Hopperstad, T. Børvik, On the Material Characterization of an Aluminium
317 Alloy Using Different Specimens and Identification Methods, 2(8) (2018) 400.
- 318 [19] User Manual - eCorr - Digital Image Correlation Tool. Available online:
319 <https://www.ntnu.edu/kt/ecorr>, 2019.
- 320 [20] Y. Chen, A.H. Clausen, O.S. Hopperstad, M. Langseth, Application of a split-Hopkinson
321 tension bar in a mutual assessment of experimental tests and numerical predictions, International
322 Journal of Impact Engineering 38(10) (2011) 824-836.

323 [21] A. Manes, R. Porcaro, H. Ilstad, E. Levold, M. Langseth, T. Børvik, The behaviour of an
324 offshore steel pipeline material subjected to bending and stretching, Ships and Offshore Structures
325 7(4) (2012) 371-387.

326

327 **Tables**

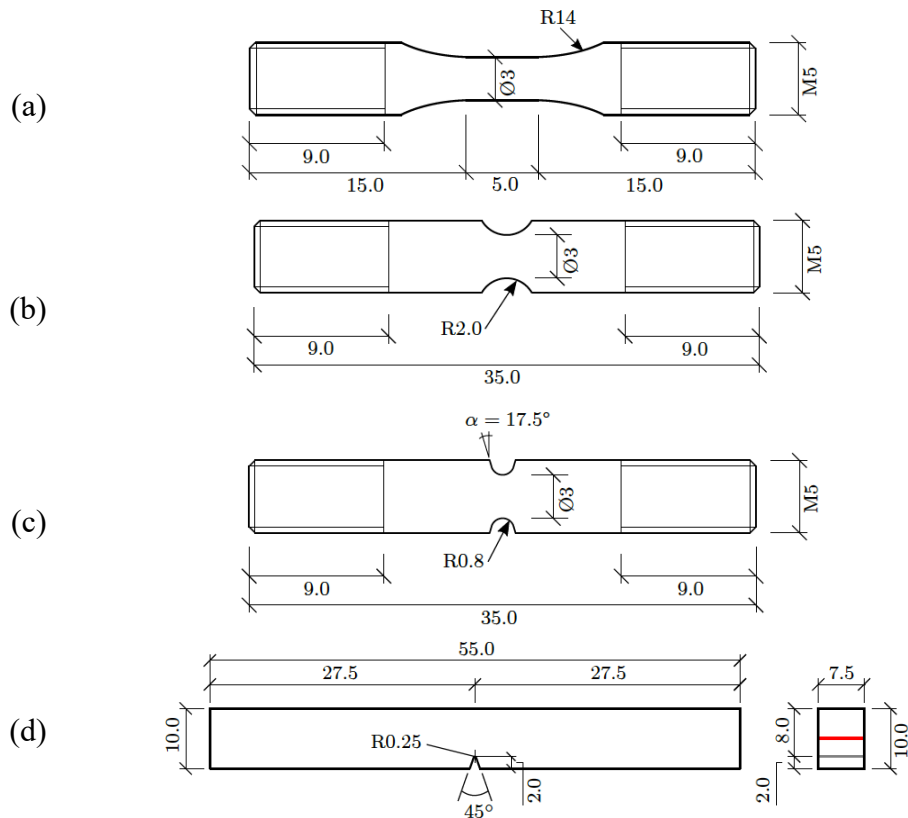
328 Table 1. Chemical composition and mechanical properties of Strenx 960 Plus steel.

Chemical composition (in weight %)															
	C	Si	Mn	P	S	Cr	Ni	Mo	V	Ti	Cu	Al	Nb	B	N
Nominal	0.18	0.50	1.70	0.020	0.010	-	-	-	-	-	-	0.018	-	-	-
Certificate	0.16	0.28	1.28	0.009	0.001	0.15	0.05	0.40	0.04	0.01	0.01	0.041	0.002	0.0015	0.003
Mechanical properties															
Yield strength		Tensile strength			Elongation			Impact properties							
R _{eH} (min MPa)		R _m (MPa)			A (min %)			T (°C)		Absorbed energy (J)					
960		980 – 1150			7			-40		27					

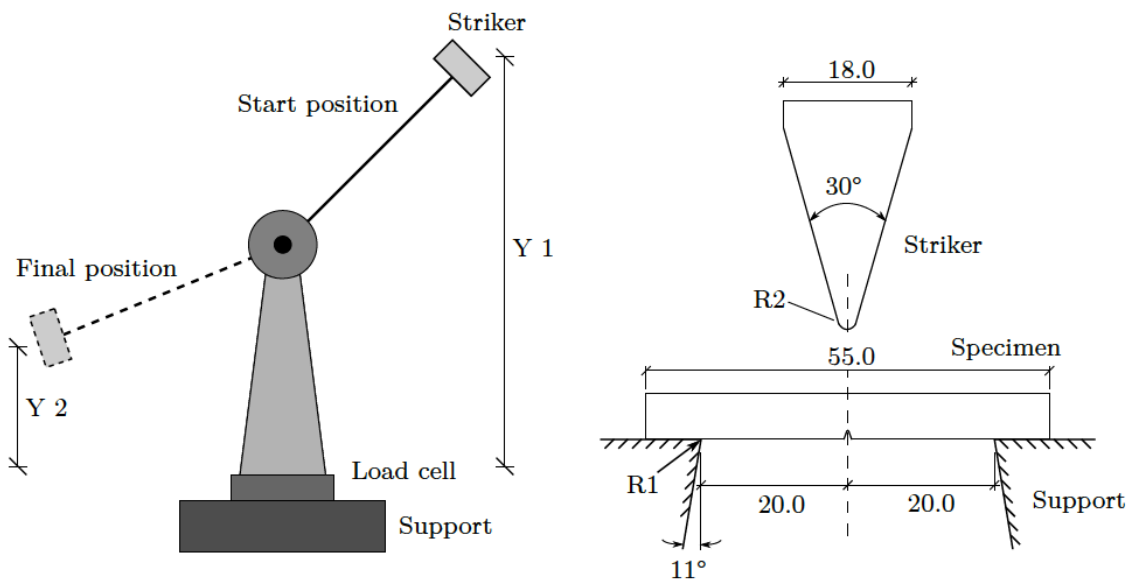
329

330

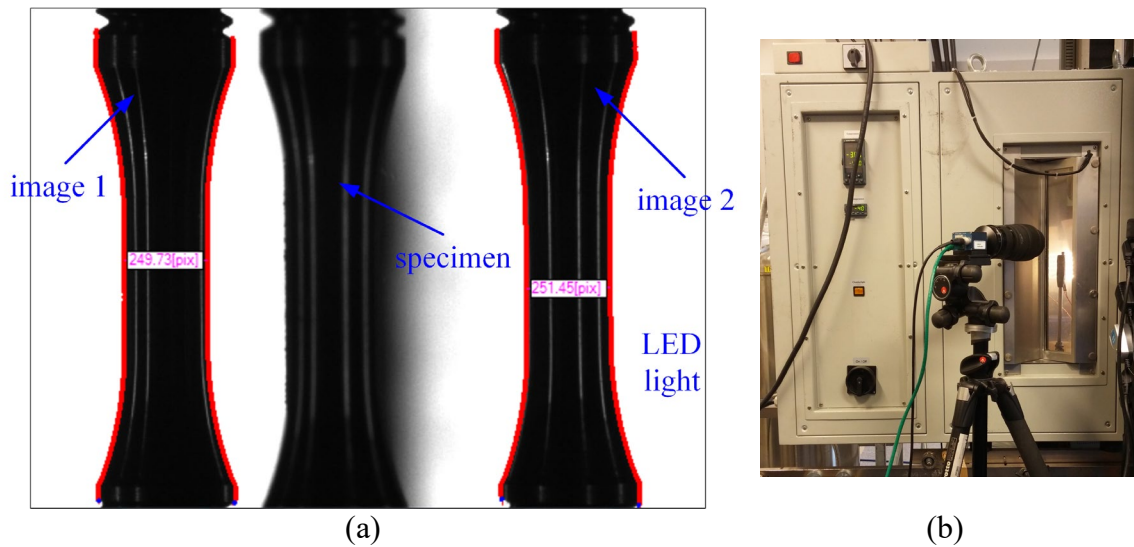
331



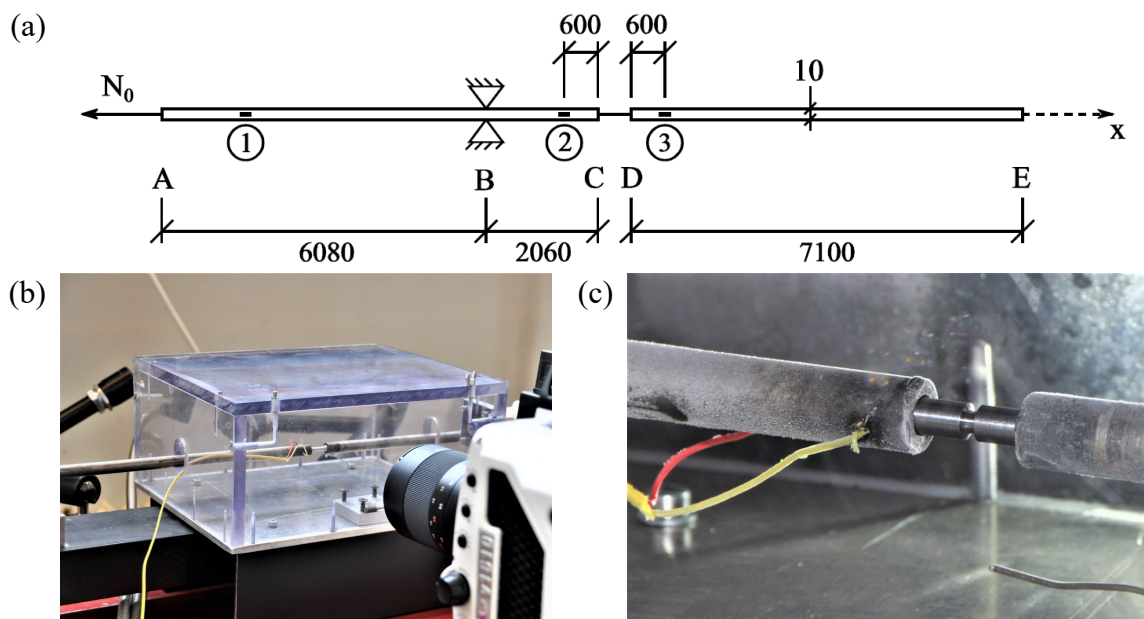
333 Figure 1. Geometries of the (a) smooth and pre-notched tension specimens with radius (b)
 334 $R = 2.0$ mm and (c) $R = 0.8$ mm, and (d) the Charpy V-notch specimen.
 335



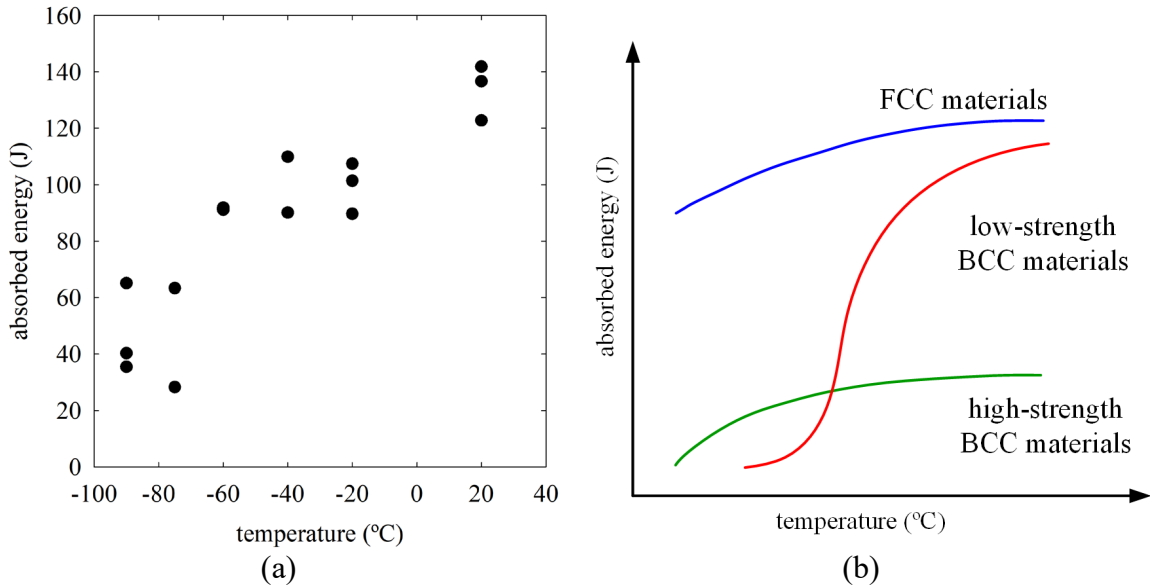
336 Figure 2. Scheme of the pendulum device and the inverse set-up used for the Charpy V-
 337 notch impact tests.
 338



339 Figure 3. (a) Illustration of the edge tracing technique used to monitor the minimum cross-
 340 section diameter of the specimen in two perpendicular directions. (b) Environmental
 341 chamber used for the low temperature tests in quasi-static regime.
 342

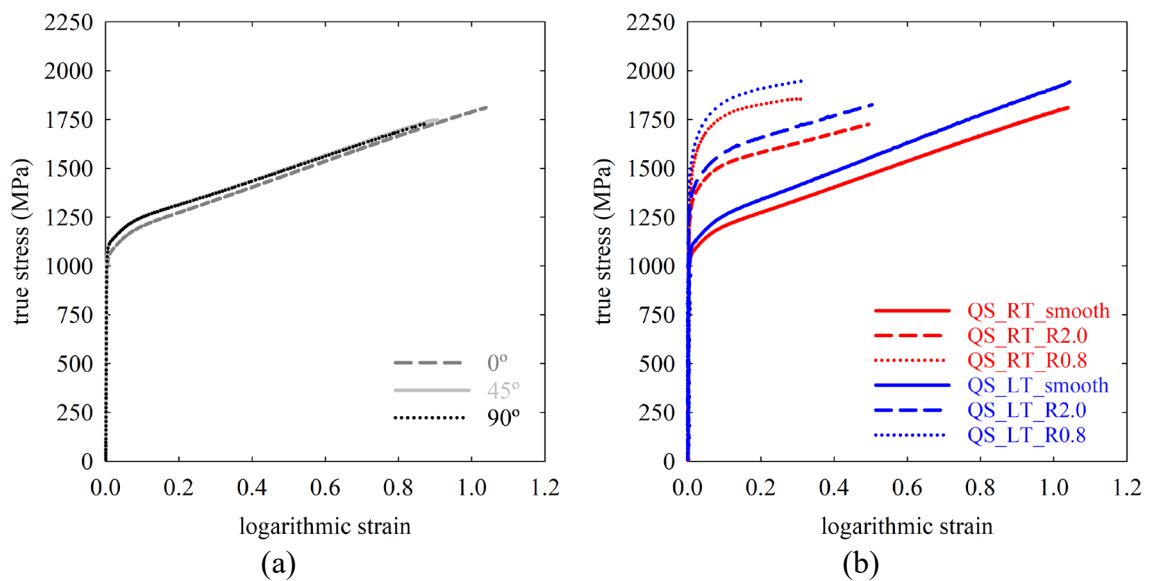


343 Figure 4. Experimental set-up of the dynamic tensile tests. (a) Schematic view of the SHTB
 344 (dimensions in mm). (b) Polycarbonate temperature chamber. (c) Specimen located in
 345 testing position. Thermocouples attached to the bars to control the sub-zero temperature.
 346

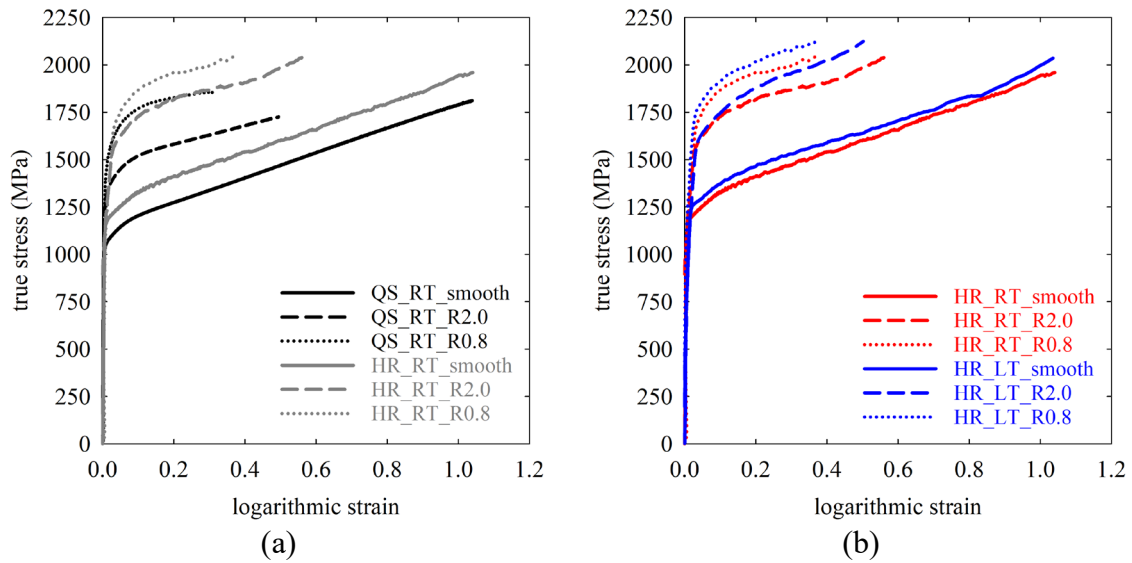


347 Figure 5. Charpy V-notch tests: (a) The absorbed energy as a function of temperature, from
 348 +20°C down to -90°C. (b) Illustration of the theoretical temperature-transition curve for
 349 different materials, adapted from Dieter [9].

350



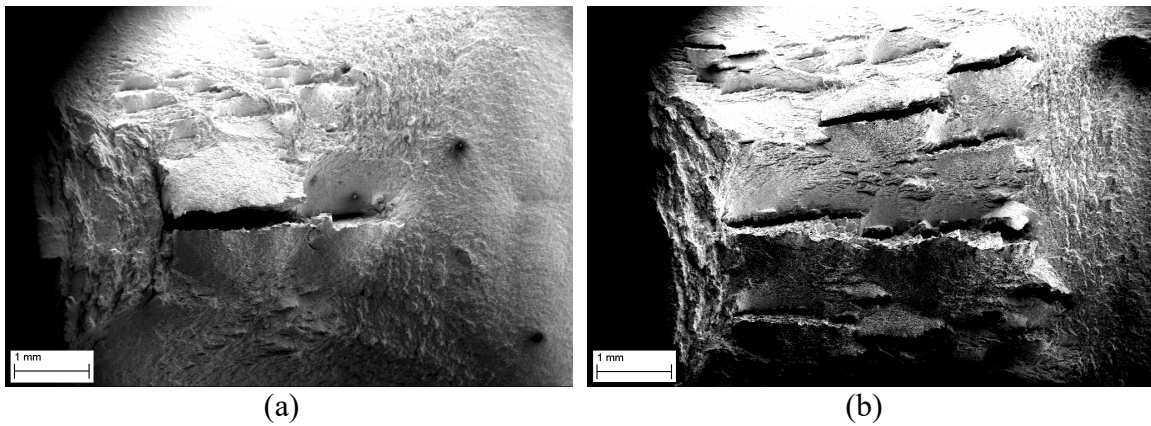
351 Figure 6. True stress-strain curves of quasi-static tests: (a) Smooth specimens extracted from
 352 0°, 45° and 90° orientations at room temperature. (b) Smooth and pre-notched specimens
 353 from 0° orientation at +20°C (in red, RT) and -40°C (in blue, LT).



354 Figure 7. (a) True stress-strain curves of both quasi-static (LR) and dynamic (HR) tensile
 355 tests at room temperature. (b) Effect of temperature on the dynamic tensile test, +20°C (in
 356 red, RT) and -40°C (in blue, LT).

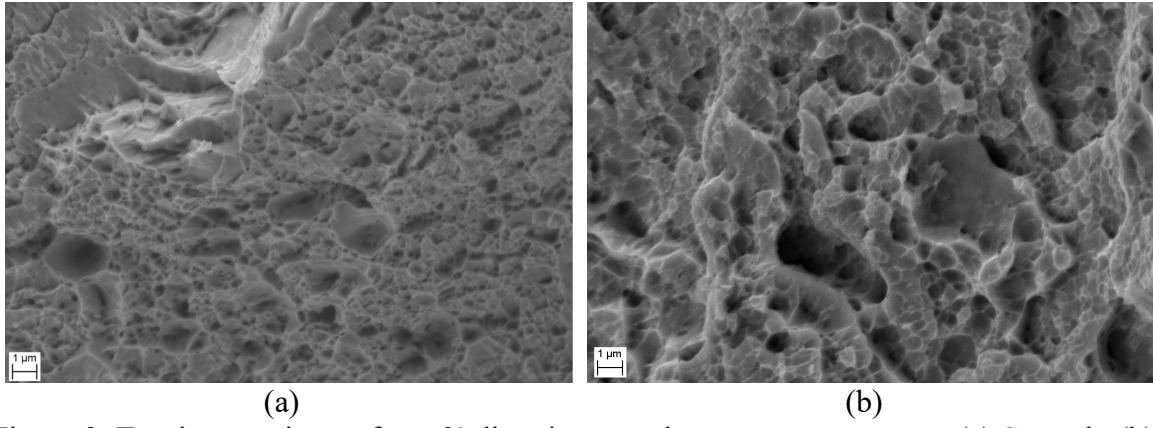
357

358

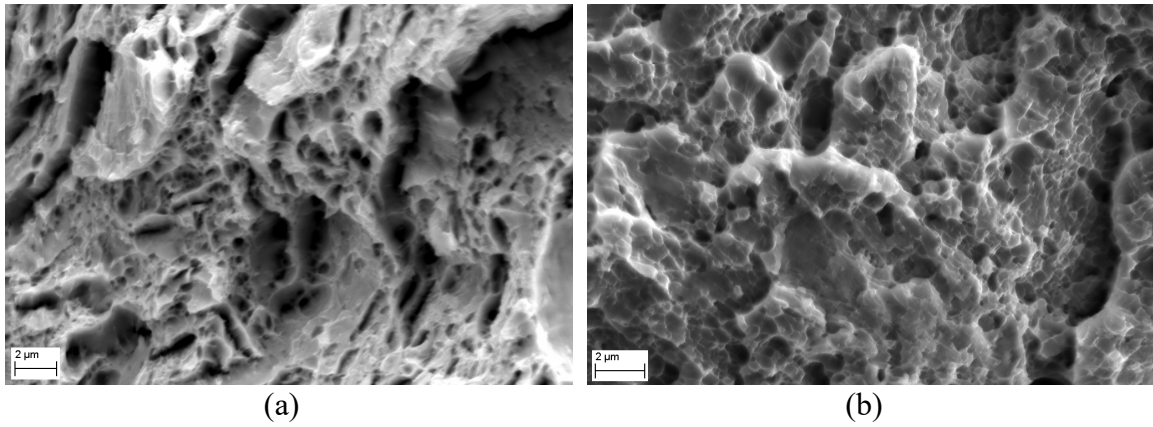


359 Figure 8. Charpy V-notch specimens: (a) Room temperature test. (b) -40°C test.

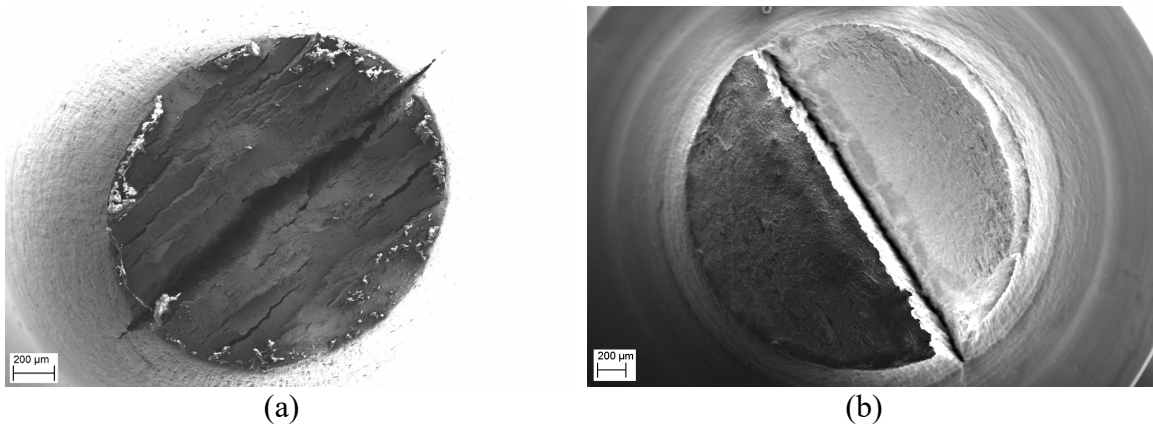
360



361 Figure 9. Tension specimens from 0° direction tested at room temperature. (a) Smooth. (b)
 362 Pre-notched with R0.8.
 363
 364



365 Figure 10. Tension specimens from 0° direction tested at -40°C. (a) Smooth. (b) Pre-notched
 366 with R0.8.
 367



368 Figure 11. Tension specimens from 0° direction tested at room temperature. (a) Smooth. (b)
 369 Pre-notched with R0.8.